Veröffentlichung

Im Rahmen des SFB 880. www.sfb880.tu-braunschweig.de

Autoren

Diekmann, Jobst Henning

Titel

Trim Analysis of Nonlinear Flight Dynamics for a Civil Aircraft with Active High-Lift System

Publisher o. Konferenz

62. Deutscher Luft- und Raumfahrtkongress, Stuttgart, 2013

Jahr

2013

Internet-Link (Doi-Nr.)

TRIM ANALYSIS OF NONLINEAR FLIGHT DYNAMICS FOR A CIVIL AIRCRAFT WITH ACTIVE HIGH-LIFT SYSTEM

J.H. Diekmann, German Aerospace Center (DLR), Institute of Flight Systems
38108 Braunschweig, Germany

Abstract

This paper shows recent flight mechanical simulation results of a civil active high-lift aircraft with blown Coandă flaps. The main focus lies on the trim analysis of the aircraft. To this end the basic structure and core elements of the nonlinear model, describing the dynamic behavior of an aircraft with this specific type of active high-lift system, are presented. The center of gravity location range allowing controllability and static stability of the aircraft is determined, followed by an analysis of the resulting characteristics of the aerodynamic model and their impact on the trim results of the aircraft. The results show specific flight mechanical difficulties due to the active high-lift system, namely characteristics hardly compatible with safe take-off and approach procedures. The physical explanations will be given and discussed. The necessity of the application of a wing leading edge device is pointed out by preliminary studies and further remedial means are proposed.

Nomenclature

C	Coefficient or derivative	-
C_μ	Jet momentum coefficient	-
ΔC_μ	Deviation from reference jet momentum	-
$C_{\mu Ref}$	Reference jet momentum coefficient	-
F	Force	N
I	Mass inertia	kgm^2
i_{HTP}	Incidence angle horizontal tailplane	°
k_1, k_2	Drag polynomial factors	-
l_μ	Mean aerodynamic chord	m
l_{Ref}	Lever arm of horizontal tailplane	m
M	Mach number	-
$m, \dot{m}$	Mass, mass flow	kg, kg/s
Ma	Mach number	-
p, q, r	Angular rates	°/s
$q_\infty, \bar{q}$	Dynamic pressure	N/m^2
$q^\star$	Dimensionless pitch rate	-
S	Main wing area	m^2
S_{HTP}	Horizontal tailplane area	m^2
t	Time	s
u_k, v_k, w_k	Aircraft velocity (inertial frame)	m/s
V	Airspeed	m/s
v_{jet}	Fluid velocity	m/s
α	Angle of attack	°
α_{HTP}	Local angle of attack horizontal tailplane	°
β	Sideslip angle	°
ε	Downwash angle	°
η	Elevator deflection	°
Φ, Θ, Ψ	Aircraft attitude angles	°
τ	Transport delay	s
ω	Angular frequency	rad/s

Indices and Superscripts

$_0$	Value for zero angle of attack
$_A$	Aerodynamic
$_{cg}$	Center of gravity
$_{C_\mu}$	Gradient w.r.t. jet momentum coefficient
$_D$	Drag
$_{dyn}$	Dynamic value due to angular rates
$_{Fl}$	Flap
$_G$	Gravity
$_{jet}$	Jet of the blowing system
$_k$	Kinetic (w.r.t. to ground)
$_L$	Lift
$_m$	Pitching moment
$_{min}$	Minimum
$_N$	Neutral Point
$_{Ref}$	Reference
$_{Stall}$	Stall Coefficient
$_\alpha$	Gradient w.r.t. angle of attack
$_\eta$	Gradient w.r.t. elevator deflection

Abbreviations

AHLS	Active High-Lift System
AoA	Angle of Attack

BLC	Boundary Layer Control
CC	Circulation Control
CFD	Computational Fluid Dynamics
CN	Clean nose
CS-25	Certification Specification 25
DN	Droop nose
EASA	European Aviation Safety Agency
HTP	Horizontal Tailplane
MAC	Mean Aerodynamic Chord
PrADO	Preliminary Aircraft Design and Optimization [tool]
RANS	Reynolds Averaged Navier Stokes [equations]
SFB	Sonderforschungsbereich (Collaborative Research Center)
SM	Static Margin
STOL	Short Takeoff and Landing
WFC	Wing/Fuselage Combination

1 Introduction

Recent air traffic forecasts predict a continuous increase of movements for civil aviation. This ultimately leads to saturation of capacities at airports as well as in airspace. A promising idea to provide more capacity without building new airports is the use of smaller already existing airports in the close vicinity of bigger cities. A medium-range aircraft for about 100 passengers with short takeoff and landing (STOL) capabilities would be able to take off and land on short runways as usually found on such small airports.

The necessary aircraft characteristics and capabilities of such a system can be achieved by an aircraft with an active high lift system (AHLS). Due to the severe impact on the whole aircraft design including aerodynamics, structure, engines and flight dynamics, the initial work in the "Sonderforschungsbereich 880" (SFB) is to create a proper aircraft design by starting with a complete development of a civil transport type aircraft. A cutaway drawing of the reference aircraft[1] can be seen in Figure 1. The main focus of attention is the AHLS, which is based on an internally blown flap system. Besides the main target of increasing lift, the new high lift system gives some additional options as well as restrictions in terms of aircraft control.

An internally blown flaps system as used for the SFB reference aircraft blows pressurized air over the knee of the so-called Coandă surface flap, which can be seen fully deflected at the trailing edge of the wing in Figure 1. This blowing system is installed along the wingspan and thus offers the chance to influence the circulation distribution over the wing with severe impact on forces and moments acting on the aircraft. As a result of the additional lift produced by the system the downwash angles decrease to larger negative values than for conventional high-lift systems. These changes in aerodynamics have an impact on other parts of the aircraft. The change in pitching moment and downwash angle strongly affects the aerodynamics of the horizontal tailplane (HTP). Besides the increase of lift and drag the system has an impact on the pitching moment of the wing by creating an additional nose down component. This additional pitching moment influences the required trimming conditions of the HTP. A strong downforce induced by the HTP is necessary to counteract the additional pitching moment induced by the AHLS in order to trim the aircraft, producing additional drag and therefore trimming losses. Even though the strong downwash keeps the trimming incidence angles of the HTP at reasonable values, a high aerodynamic effectiveness of the HTP is crucial.

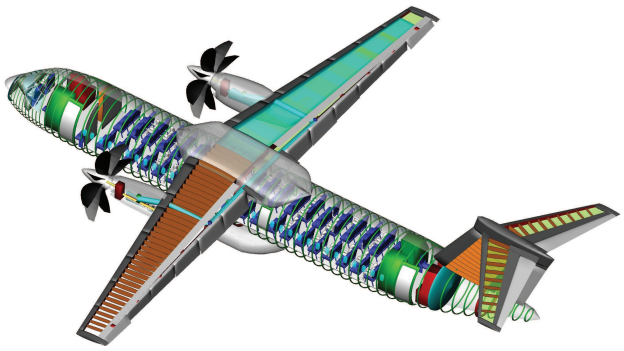

Figure 1: Cutaway drawing of the SFB 880 reference aircraft configuration

For analysis of the mentioned flight mechanical difficulties due to the AHLS a flight mechanical simulation model for the longitudinal motion of such an AHLS supported aircraft has been developed. The following sections will describe the development of the simulation and will give results from static stability analysis as well as trim investigations for different flap configurations. A preliminary further development of the configuration will be investigated and discussed.

[1] created by Tayson Weiss, Institute of Aircraft Design and Lightweight Structures (IFL), TU Braunschweig

2 Simulation Model Design

In order to be able to simulate the longitudinal motion of an active high lift supported aircraft a flight dynamics model has to be established. The model should describe all direct and indirect influences on aircraft dynamics. This includes the main effects like aerodynamics and engines, but also other subsystems like actuator dynamics or gear influences as well as cross couplings between the various subsystems. The simulations are performed by using MATLAB/Simulink[2], which allows a combination of script based and block diagram modeling. Figure 2 shows the basic structure of the simulation model. As a source for general aircraft data the reference aircraft data generated by PrADO are used (see [1]). This database provides information about geometry, weight, moments of inertia and engine characteristics of the aircraft. The aerodynamic coefficients are identified from CFD results provided by SFB partner projects (see [2]).

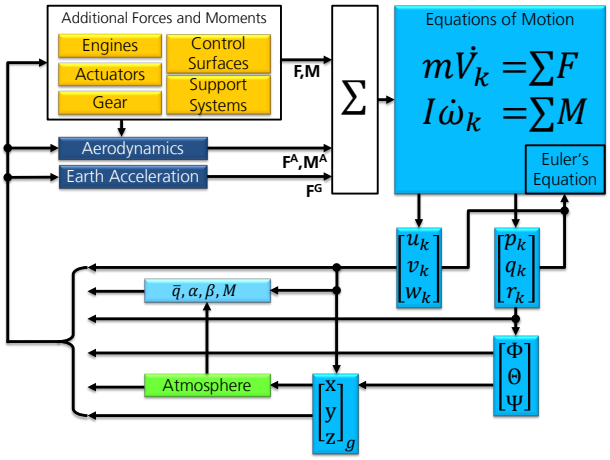

Figure 2: Block diagram showing the model structure of the flight dynamical model including major forces and moments, the equations of motion and the resulting movement of the aircraft, which is fed back to the forces and moments models

For conventional flap systems the airflow along the airfoil tends to separate from the flap once a maximum flap deflection is exceeded. Active high-lift is characterized by using pressurized blowing air or sucking air to increase the lift of an airfoil. The basic function of the blown Coandă flap system used here is to preserve the lift increasing effect of the flap even for extremely high flap deflections. The superimposed airstream of the blown flap is injected into the boundary layer at the knee of the flap. This keeps the airflow attached to the flap even for higher flap deflections and thus enhances the performance of the flap system. Contrary to other lift enhancing systems which use the whole jetstream of the engines to influence the wing's aerodynamics (e.g. Upper Surface Blowing, USB), the Coandă concept system requires a much smaller air mass flow to achieve a higher lift performance (see [3] and [4]). This leads to a high efficiency of the system in the sense of additional lift to aircraft energy investment ratio. The efficiency of the AHLS can be divided into two sections, depending on the jet momentum of the system. The jet momentum coefficient is defined in Equation 1.

$$C_\mu = \frac{\dot{m}_{jet} \cdot v_{jet}}{q_\infty \cdot S} \tag{1}$$

In the Boundary Layer Control (BLC) section the injected mass flow influences the boundary layer at the flap, whereas in the Circulation Control (CC) section new circulation is induced by the strong jetstream of the blowing system. The BLC section has its minimum value defined by the point of flow separation from the flap. The model is based on CFD results which clearly indicate the characteristic of two different gradients for the two sections, cf. Figure 3. A reference value ($C_{\mu Ref}$) has been defined which indicates the maximum value of the BLC section and the minimum value for the circulation control section. The findings of the CFD analysis are confirmed in [5]. Below the minimum value $C_{\mu min}$ the flow along the flap can be considered to be separated.

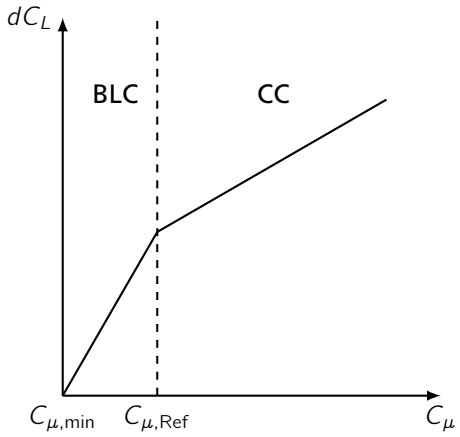

Figure 3: Lift increase for different jet momentum coefficients (C_μ) in the Boundary Layer Control (BLC) and Circulation Control (CC) area [6]

For CFD calculations DLR's Tau code [7] employing Reynolds Averaged Navier Stokes equations (RANS)

[2] by MathWorks

and the commercial tool VSAero[3] based on panel methods have been used. Aerodynamic data for the wing/fuselage combination (WFC) in clean configuration and the horizontal tailplane (HTP) have been created by the low fidelity CFD tool VSAero whereas the complex aerodynamics of the WFC in full flaps configuration with AHLS have been calculated with the high fidelity Tau code.

The underlying aerodynamic model consists of a dimensionless coefficient model which has been determined by the analysis of the CFD data. A two-point modeling approach has been used by separating the aerodynamics of the WFC from the aerodynamics of the HTP as in Equation 2.

$$(2)\quad C_L = C_{L,WFC}(\alpha, C_\mu) + \frac{S_{HTP}}{S} \cdot C_{L,HTP}(\alpha_{HTP}, \eta)$$

The lift of the WFC has been modeled by a standard lift model ($C_{L,WFC}(\alpha)$) including the lift for zero angle of attack (AoA, α) and a lift curve slope versus angle of attack ($C_{L\alpha}$). Additional lift increments have been determined for the deflected flap at reference jet momentum ($\delta C_{L,FI,C_{\mu Ref}}(\alpha)$), the variation of the jet momentum ($\delta C_{L,C_\mu}(\alpha, \Delta C_\mu)$) and the stall effect ($C_{L,Stall}(\alpha, C_\mu)$), which is also dependent on the jet momentum of the AHLS.

$$\begin{aligned}(3)\quad C_{L,WFC}(\alpha, C_\mu) = {} & C_{L,WFC}(\alpha) + \delta C_{L,FI,C_{\mu Ref}}(\alpha) \\ & + \delta C_{L,C_\mu}(\alpha, \Delta C_\mu) \\ & - C_{L,Stall}(\alpha, C_\mu)\end{aligned}$$

Beside the usual dependency on AoA the resulting model has a strong dependency on the setting of the AHLS by the jet momentum coefficient. Figure 4 shows the resulting lift slopes versus AoA. The underlying CFD data points have been inserted as boxes. The shaded area is the BLC section which will be used as the preferred target area to operate the aircraft in.

The lift of the HTP is coupled to the lift of the WFC by the resulting downwash which affects the local AoA (α_{HTP}) at the position of the HTP, which is reflected by Equation 4.

$$\begin{aligned}(4)\quad C_{L,HTP}(\alpha_{HTP}, \eta) = {} & C_{L\alpha,HTP} \cdot \alpha_{HTP}(C_{L,WFC}, C_\mu) \\ & + C_{L,\eta} \cdot \eta\end{aligned}$$

Therefore a downwash (ε) model has been developed which describes the influence of the WFC lift, the transport delay (τ) for lift changes at the WFC until it affects the lift of the HTP as well as a jet momentum correction taking into account the varying lift distribution along the wingspan due to the optimized AHLS settings. Given AoA, incidence angle (i_{HTP}) as the control input for trimming the HTP and the dynamic AoA (α_{dyn}) resulting from pitch rates around the center of gravity, the local AoA can be calculated as in Equation 5.

$$\begin{aligned}(5)\quad \alpha_{HTP}(C_{L,WFC}, C_\mu) = {} & \alpha + \varepsilon(C_{L,WFC}(t-\tau), C_\mu) \\ & + i_{HTP} + \alpha_{dyn}\end{aligned}$$

The drag is modeled with a second order polynomial which can be divided into parasite drag (C_{D0}) and induced drag (C_{Di}) produced by the aircraft's lift. For the influence of the deflected flap with the blowing system at reference jet momentum ($\delta C_{D,FI,C_{\mu Ref}}$) and the variation of jet momentum ($\delta C_{D,FI,C_\mu} \cdot \Delta C_\mu$) respective increments have been added.

$$\begin{aligned}(6)\quad C_D = {} & \underbrace{C_{D0,WFC} + C_{D0,HTP}}_{C_{D0}} + \underbrace{k_1 \cdot C_L + k_2 \cdot C_L^2}_{C_{Di}} \\ & + \delta C_{D,FI,C_{\mu Ref}} \\ & + \delta C_{D,FI,C_\mu} \cdot \Delta C_\mu\end{aligned}$$

The resulting drag for the full flap configuration can be seen in Figure 5. It is obvious that the model does not describe the CFD data beyond stall. The model has not been adapted for this area as it is not the target area to operate the aircraft in, and the CFD data quality is reduced due to a lower convergence of the results. Thus the drag model follows the lift model without correction beyond stall.

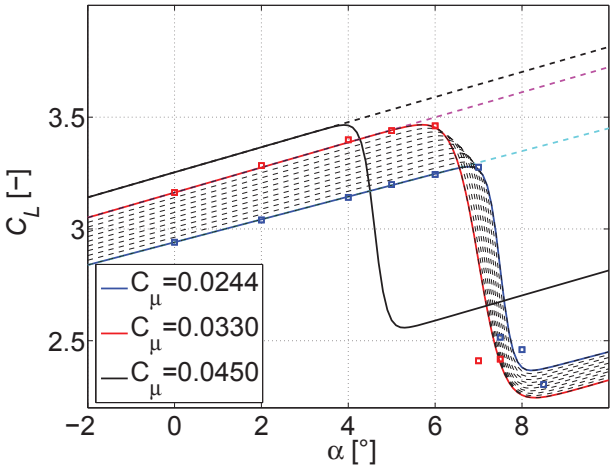

Figure 4: Nonlinear model for lift of the WFC versus AoA for different jet momentum coefficients (C_μ) including the corresponding CFD data (boxes), the linear model (dashed lines) and the preferred BLC area for system operation (shaded area)

[3] by Analytical Methods Inc.

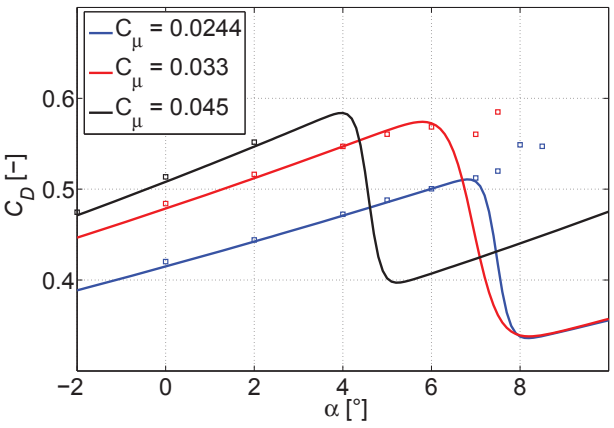

Figure 5: Nonlinear Model for drag versus AoA for different jet momentum coefficients (C_μ) including the corresponding CFD data (boxes)

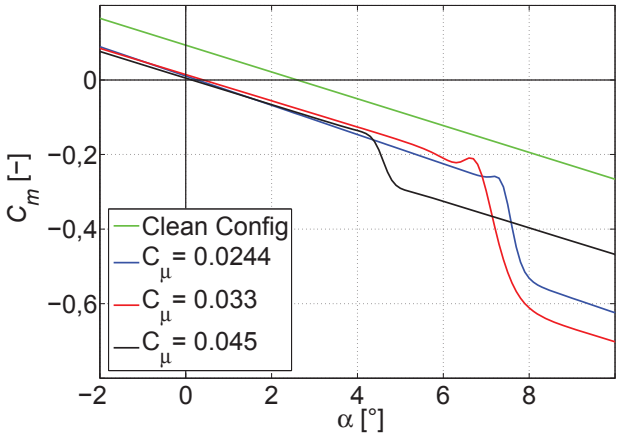

Figure 6: Nonlinear Model for pitching moment versus AoA for different jet momentum coefficients including the pitching moment in clean configuration (green line)

Similar to the lift model the pitching moment has been modeled as a two-point model, by separating the pitching moment of the WFC and the HTP. This leaves the opportunity to model the HTP pitching moment as the lift force of the HTP multiplied with the lever arm between moment reference point of the WFC and the neutral point of the HTP (l_{Ref}). The increments for the AHLS influence ($\delta C_{m,FI,C_{\mu Ref}}(\alpha), \delta C_{m,C_\mu}(\alpha, C_\mu)$) and stall ($C_{m,Stall}(\alpha, C_\mu)$) have been added as well as the dynamic reaction on pitch rates by the pitch damping ($C_{mq^\star,WFC}$). The determined model output for the pitching moment of the full aircraft is presented in Figure 6.

$$
\begin{aligned}
(7)\quad C_m(\alpha, C_\mu) &= C_{m0,WFC} + C_{m\alpha,WFC}\cdot(\alpha) \\
&+ \delta C_{m,FI,C_{\mu Ref}}(\alpha) + \delta C_{m,C_\mu}(\alpha, C_\mu) \\
&- C_{m,Stall}(\alpha, C_\mu) \\
&+ C_{mq^\star,WFC}\cdot q^\star \\
&\underbrace{- \frac{S_{HTP}}{S}\cdot\frac{l_{Ref}}{l_\mu}\cdot C_{L,HTP}}_{C_{m,HTP}}
\end{aligned}
$$

All AoA dependent coefficients have been corrected by a Prandt-Glauert correction factor (see [8]) multiplied to the respective coefficients in order to take Mach number effects on aerodynamics into consideration. The factor is given in Equation 8 where the mach number of the CFD analyses ($Ma_{CFD} = 0.15$) is used as reference mach number.

$$
(8)\qquad f_{PG} = \frac{\sqrt{1 - Ma_{CFD}^2}}{\sqrt{1 - Ma^2}}
$$

Apart from the expected increases in lift coefficient values, several additional coherences appeared which are only described briefly. For the operative AHLS the CFD analyses showed a very abrupt leading edge stall behavior appearing already at low AoA. Another finding was that the flap system produces a remarkably high drag even in addition to the high induced drag due to high lift coefficients. Further a great suction peak at the trailing edge due to AHLS leads to strong nose down pitching moments. The downwash of the WFC is far beyond the ordinary at high negative deflection values compared to conventional aircraft in full flaps configuration. A thorough description and discussion of these effects is given in [9]. Detailed descriptions of the underlying aerodynamic model and specific values for the coefficients can be found in [10].

The present aerodynamic model is capable to describe the effects of the AHLS. Anyhow, there are still additional influences which have to be implemented in the model, as the aircraft is designed to be powered by turboprop engines. Therefore further extensions to the recent model will be the implementation of slipstream influences of the turboprop engines on aerodynamics as well as leading edge device aerodynamics. The latter will be introduced later on in this paper.

3 Center of Gravity Locations

The center of gravity location is of major importance for the static stability of the aircraft and its controllability in the longitudinal motion. The static margin, described in Equation 9, has been determined in order to analyse the static stability of the aircraft (SM, see [11]). A good static stabil-

ity is reflected by negative static margins below $SM < -0.1$.

$$SM = \frac{C_{m\alpha}}{C_{L\alpha}} = -\frac{X_N - X_{cg}}{l_\mu} \tag{9}$$

A trim analysis has been performed for an investigation of the static margin and the controllability of the aircraft in full flaps configuration. Therefore the wing area of the HTP (S_{HTP}) and location of the center of gravity (x_{cg}) have been varied to find the forward controllability boundary and the rearward static stability boundary. Within these bounds the aircraft can be considered as statically stable and controllable in the longitudinal motion. Figure 7 shows the results of the investigation.

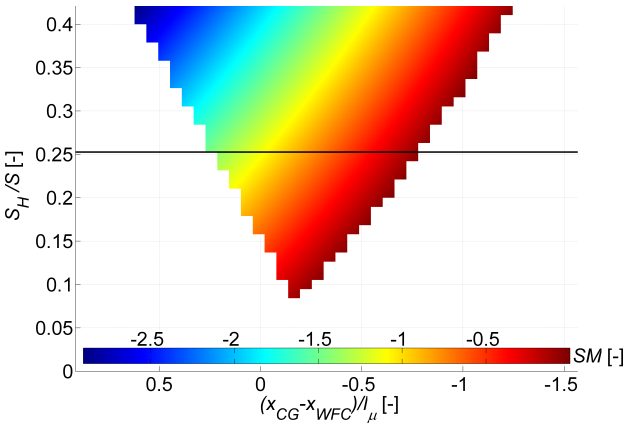

Figure 7: Static margin (SM) for different HTP to wing area ratios (S_H/S) and dimensionless center of gravity locations w.r.t. neutral point of the WFC ($(x_{CG} - x_{WFC})/l_\mu$) including the current aircraft design HTP to wing area ratio (black line)

The trim calculations for this figure have been performed for an airspeed close to stall speed ($V_{Trim} = 49\ \frac{\text{m}}{\text{s}}$) and a near ground altitude ($Alt_{Trim} = 50$ m). The HTP surface area has been varied between $0\ \text{m}^2 < S_{HTP} < 40\ \text{m}^2$ and the location of center of gravity has been varied from ($-1.5 < (x_{cg} - x_{WFC})/l_\mu < 1$). The forward boundary is defined as the first trimmable x_{cg}, whereas the the rearward boundary is given by the rearmost x_{cg} in which the aircraft remains statically stable ($C_{m\alpha} < 0$). The black horizontal line gives the surface area ratio $\frac{S_{HTP}}{S} = 0.253$ which is currently used for the SFB aircraft configuration. For this ratio a practically usable range for center of gravity locations can be achieved. Even after application of safety margins of 10% the aircraft is controllable and statically stable for center of gravity locations between $-10\%\ MAC < CG < 60\%\ MAC$. For the following trim envelope research a medium value of this range has been taken ($x_{cg,trim} = 13.8$ m $\hat{=}\ 19.5\%\ MAC$). Additional center of gravity investigations will be necessary especially in order to evaluate the controllability boundaries for several flight cases and AHLS conditions. Unfortunately these investigations cannot be subject of this paper as its focus lies on the trimmability of the aircraft.

4 Trim Configurations

The initial test for a new flight mechanical simulation model is the trimming of the aircraft. The aim is to find steady states in which the aircraft can be operated for a given condition e.g. the standard case of straight unaccelerated horizontal flight. These cases define the set of requirements for states and output values, which have to be fulfilled by adapting an equal number of input and state derivative variables. A field of trim points has been calculated this way for unaccelerated horizontal flight at different airspeeds and altitudes, as this flight case determines the envelope for the aircraft. For this calculation variable values among others are AoA, throttle setting and the incidence angle of the horizontal tailplane. The flight envelope thus found only determines the points in which the simulation model is trimmable. Additional boundaries (e.g. structural failure due to high dynamic pressures) have been applied to the trimming results afterwards.

Beside the trimmability itself, the values of the trim variables and the resulting local AoA at the horizontal tailplane are of special interest for the evaluation of the data. Table 1 gives the used aircraft masses for Maximum Take-Off Weight (MTOW), Maximum Landing Weight (MLW) and the Operating Weight Empty (OWE). (The latter is given for the sake of completeness as the extreme values of aircraft weight define the minimum envelopes.) All trim points have been calculated for the chosen center of gravity of $x_{cg,trim} = 13.8$ m $\hat{=}\ 19.5\%\ MAC$ as a middle location within the range described in Section 3, preserving a good static margin for all configurations in order to ensure comparability of the results.

MTOW	MLW	OWE
40641 kg	38901 kg	24061 kg

Table 1: Aircraft Masses

The trim investigations have been performed for different combinations of flap configurations and

aircraft masses. The clean configuration has been tested for MTOW as it would be suitable for cruise situations. Figure 8 shows the resulting envelope of this cruise configuration. A color coding indicates the trimmed values for the AoA at the respective trim point. The lift boundary can be observed on the left side of the field where the color coding indicates the highest AoA. For high altitudes the engine performance limits the envelope. The right side of the envelope at high airspeed is limited by the maximum permissible dynamic pressure and Mach number.

At this stage of the aircraft development these boundaries have to be defined arbitrarily as there is no flight test data or structural information yet. Hence mach number has been restricted to $M = 0.84$ and dynamic pressure has been limited to $p_\infty = 101325$ N/m^2. The trim envelope shows the wide range in which the cruise configured aircraft can be operated in unaccelerated horizontal flight at MTOW. The maximum altitudes as well as the high airspeed which can be achieved in this configuration are remarkable for a turboprop engine powered aircraft. This observation can be attributed to the relatively powerful engines compared to conventional aircraft. The sizing of the engines is related to the necessary climb performance during take-off phase: The bleed air extraction increases the necessary engine power as the AHLS still needs to be supplied with a sufficiently high air mass flow with one engine inoperative. The extraordinary sizing of the engines normally leads to an increased fuel consumption, which in this case is counteracted by the reduction of weight and drag due to optimization in WFC design.

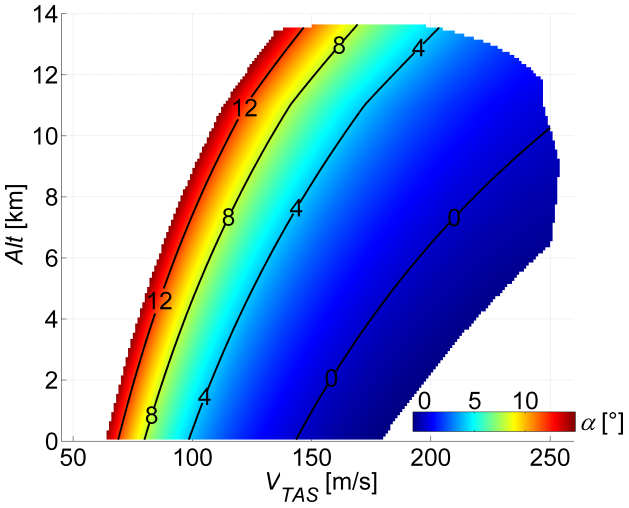

Figure 8: Envelope for cruise configuration with MTOW including the corresponding AoA

The second trim envelope presented in Figure 9 has been established for the full flaps configuration ($\delta_{Flap} = 65°$) and with active blowing system at the upper boundary of the BLC range ($C_\mu = C_{\mu,Ref} = 0.033$). This flap setting will be used for approach situations only, which justifies the analysis of the trim envelope for MLW and limiting the investigated altitude to $Alt_{max} = 7000$ m. Additionally the corresponding section of the MLW Cruise configuration envelope is presented.

The color coding shows that the majority of the trimmed AoA is of negative value. The high lift of the active high lift enhanced flap system is achieved at very low AoA. In combination with a rather flat lift slope with respect to AoA this requires strong changes in AoA for an increase of airspeed.

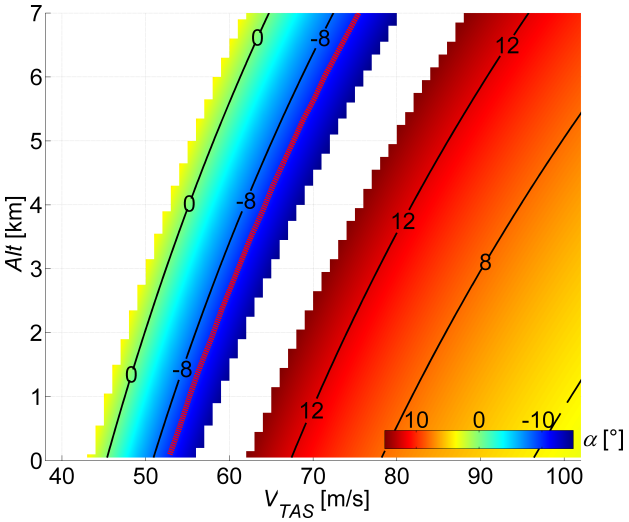

Figure 9: Detail view of the envelope for approach (left) compared to cruise configuration (right) with MLW including the corresponding AoA and allowed minimum approach speed (red line)

In order to perform a smooth transition from one flap setting to the other it is necessary that the corresponding envelopes have a reasonable intersection in airspeed and altitude. As the envelopes for cruise and approach do not intersect, a direct transition is not possible. This finding is neither extraordinary nor specific for AHLS aircraft as many conventional aircraft have several intermediate flap settings between cruise and approach configuration too. The remarkable point in the comparison of the two envelopes is the large discrepancy in AoA between the high speed boundary of the approach configuration and the low speed boundary of the cruise configuration of nearly $\Delta\alpha = 30°$. The approach configuration envelope shows that with

increasing airspeed even slightly above stall speed the AoA for a trimmed unaccelerated horizontal flight has to be negative. Furthermore near ground an increase of airspeed of only $\Delta V_{TAS} \approx 15\frac{m}{s}$ leads to large negative AoA below $\alpha < -10°$. It has to be noted that a horizontal flight is a simplified case as the aircraft will be in a descent during most of the approach phase, see below later.

The purpose of the AHLS at maximum performance is to achieve very low airspeeds during approach situations. The great advantage especially of this aircraft is the ability to fly at very low speeds and with large drag values, which allows to perform steeper approaches than standard ($\gamma < -3°$). These approaches are likely to reduce the noise exposition of the local community, an important aspect when using small airfields in suburban areas as mentioned at the beginning in Section 1.

Without wind influence pitch attitude can be defined as $\Theta = \alpha + \gamma$. This means that the aircraft would arrive on the ground with a large negative pitch attitude (for steep approaches even more pronounced). Thus the nose gear would hit the ground first if this attitude is not strongly increased by extreme flare maneuvers, which in turn would increase the risk of stall. As a consequence, the desired pitch attitude during approach should be positive as the case of a missed flare maneuver has to be considered. Even though it would be theoretically possible to reach neutral pitch attitude if flying very closely to stall speed and with a very moderate flight path angle this is not a realistic or relevant case. The required range for AoA during approach for a minimum flight path angle value of $\gamma = -3°$ would be between $3° < \alpha_{Approach} \leq 10°$. This also assumes an upper boundary for pitch attitude given by the risk of tail strike ($\Theta_{Tailstrike} = 8.19°$).

The Certification Specification 25 (CS-25, [12]) issued by the European Aviation Safety Agency (EASA) defines the minimum approach speed as in Equation 10.

$$V_{min,Approach} = 1.23 \cdot V_{Stall} \tag{10}$$

The red line in Figure 9 indicates the minimum approach speed for the given envelope. According to the requirement for $V_{min,Approach}$ the resulting AoA during approach phase would have to be below $\alpha < -10°$. It is obvious that this full flap setting does not seem to meet CS-25 in large parts of the envelope. The remaining airspeed range might even be exceeded by wind or gust so that the aircraft is likely leave the envelope unintentionally. Usually aircraft manufacturers address this matter in the aircraft operations manual by additional airspeed safety margins for given wind and gust level. As STOL aircraft already operate at very low airspeed, strong wind components can become even more important than for conventional aircraft.

Additional attention needs to be paid to the enormous nose down pitching moments which have to be trimmed by the HTP. The center of gravity location plays an important role in this respect, which can be recognized when looking at the specific values of the trim points given in Table 2. For these data sets the aircraft has been trimmed for an airspeed close to stall speed and another airspeed slightly above minimum approach speed. The jet momentum has been set to the maximum performance of $C_\mu = 0.045$ as this leads to the maximum pitching moment of the WFC which needs to be trimmed. For comparison reasons the same values have been trimmed for location "A" $x_{CG,A} = 19.5\%\ MAC$ which was used for the trim envelopes and a more forward location "B" at $x_{CG,B} = 0\%\ MAC$. The values show that a movement of the center of gravity of only $19.5\%\ MAC \approx 0.7\ m$ has an enormous effect on the loading of the HTP, which is reflected by the necessary local AoA to trim the aircraft. A remarkable aspect is the large deflection of the HTP for location A which is necessary to neutralize the downwash angle. This aspect has to be considered when the deflection range is defined. For the center of gravity in location B the loading of the HTP increases rapidly. In order to avoid tail stall effects, the center of gravity location should not be pushed any further forward. It is necessary to preserve enough margin in AoA of the HTP so that sufficient pitch control can be guaranteed. Due to the required down force a negatively cambered profile could reduce the necessary local AoA for the HTP without increasing the surface area. The reasonable range for center of gravity locations indicates that the surface area of the HTP seems to be sufficient.

V_{TAS} $\left[\frac{m}{s}\right]$		x_{CG} [% MAC]	α [°]	i_{HTP} [°]	α_{HTP} [°]
44	V_{Stall}	0.0	3.4	0.0	−7.62
54	V_{min}	0.0	−11.4	6.58	−10.54
44	V_{Stall}	19.5	1.8	9.8	0.0
54	V_{min}	19.5	−12.5	13.0	−0.1

Table 2: Approach configuration trim points for $C_\mu = 0.045$

The described disadvantage of large negative AoA,

however, definitely invalidates this configuration for operational application. The design has to be considered to be impractical for civil aircraft operation unless adapted adequately. As mitigation the installation of a leading edge device means a droop nose has been investigated. Recent SFB880 results addressing this topic potentially can contribute to resolve this disadvantage. The results will be introduced and applied to the simulation model aerodynamics in the next section.

5 Droop Nose Integration

One of the most promising solutions for the difficulties created by the AHLS is the application of a leading edge device like slats or a droop nose as used in this case. These are well known devices cause an increase of maximum AoA and lift coefficient leading to a reduced stall speed and minimum approach speeds at higher AoA and thus might increase the resulting pitch attitudes during the approach of the AHLS aircraft to values comparable to those of conventional civil aircraft. A 2D CFD analysis for a wing profile with AHLS and droop nose application has been performed [13]. The results of this analysis show the expected improvement in terms of maximum AoA increase, as can be seen in Figure 10. The enormous potential of the leading edge device is obvious, although it has to be noted that there will be induced losses for the transformation to 3D aerodynamics. The major effect of the droop nose (DN) becomes clear when looking at the chordwise pressure distributions in Figure 11. The basic reason for the early leading edge stall of the wing profile with clean nose (CN) at small angles of attack are the large negative values of the suction peak at the leading edge of the profile. This is due to the high flow velocities induced in forward direction by the AHLS at the profile trailing edge. This large negative pressure leads to an early leading edge flow separation at low angles of attack. The DN reduces the leading edge pressure values and creates an expanded distribution of the suction along the profile. Thus the flow separation starts later with the pressure value increasing at larger angles of attack.

In order to demonstrate the potential of the DN application to the wing, a preliminary extension of the aerodynamic model has been developed. Considering that the results of the 2D CFD analysis are not directly applicable to the model which is based on 3D CFD data, as a first step only lift slope and pitching moment slope ratios (Equation 11&12) as well as the increase in AoA (Equation 13) have been

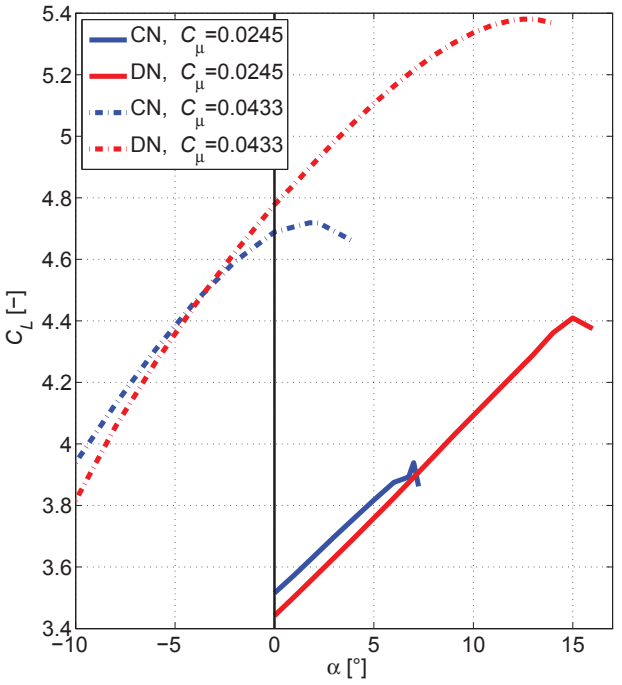

Figure 10: Lift increase due to droop nose (DN, red) compared to clean nose (CN, blue) for a jet momentum in BLC ($C_\mu = 0.0245$, full line) and CC ($C_\mu = 0.0433$, dash-dot) areas

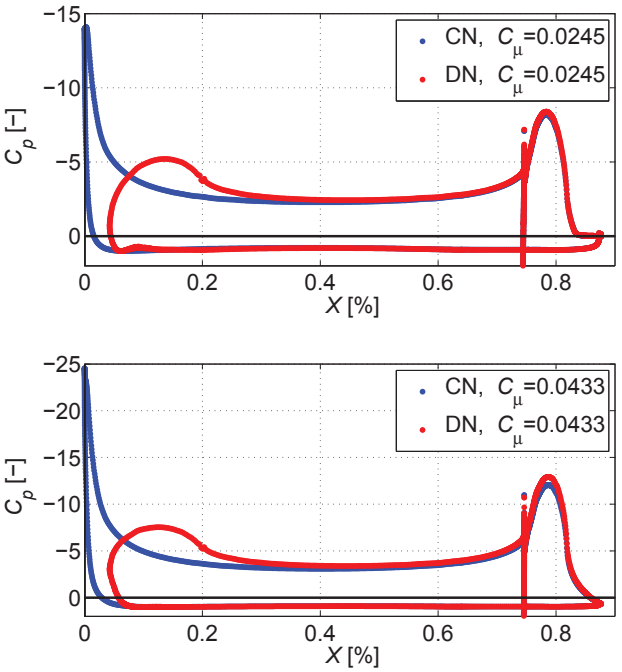

Figure 11: Droop nose effect (DN) on pressure distribution (c_p) along wing chord (X) compared to clean nose (CN) for a jet momentum in BLC ($C_\mu = 0.0245$) and CC ($C_\mu = 0.0433$) areas

converted.

$$C_{L\alpha,DN,3D} = C_{L\alpha,CN,3D} \cdot f_{L\alpha,2D}(C_\mu) = C_{L\alpha,CN,3D} \cdot \left(\frac{C_{L\alpha,DN,2D}(C_\mu)}{C_{L\alpha,CN,2D}(C_\mu)} \right) \tag{11}$$

$$C_{m\alpha,DN,3D} = C_{m\alpha,CN,3D} \cdot f_{m\alpha,2D}(C_\mu) = C_{m\alpha,CN,3D} \cdot \left(\frac{C_{m\alpha,DN,2D}(C_\mu)}{C_{m\alpha,CN,2D}(C_\mu)} \right) \tag{12}$$

$$\alpha_{max,DN,3D} = \alpha_{max,DN,3D} + \Delta\alpha_{max,2D}(C_\mu) = \alpha_{max,CN,3D} + \alpha_{max,DN,2D}(C_\mu) - \alpha_{max,CN,2D}(C_\mu) \tag{13}$$

These adaptions of the model lead to a different behavior in the resulting trim envelope. The most relevant impacts can be observed for jet momentum coefficient values in the CC range. For this range the DN influence on lift slope is considerably increased compared to the influences in BLC range. The maximum AoA increment is larger for the CC range than for the BLC range. The following Figure 12 shows the changes in the calculated envelope for a jet momentum in the CC range ($C_\mu = 0.045$), where the same limitations are applied as for the approach configuration envelope in Section 4.

The first aspect which catches the eye is the widely increased airspeed range in which the aircraft can be operated. It is also obvious that the gap between the cruise and the approach configurations disappeared with the droop nose integration. Even though the AoA still differs extremely at the intersection, this aspect increases the chance that with an intermediate flap setting a smooth transition between the configurations becomes feasible. A second aspect is the intended increase in AoA. This appearance differs to resulting envelopes in BLC range as the corresponding envelope does not close the gap to cruise configuration completely (not depicted). This is quite remarkable as for the CN wing a reduction in jet momentum directly led to the ability to push the AoA limits to higher airspeeds. The enormous performance increase of the AHLS in CC range arises from the steepening influence of the DN on the lift curve gradients. With CN this gradient tends to be remarkably shallow for the AHLS WFC, which leads to great reductions in AoA, for small lift coefficient reductions are necessary to trim the aircraft for increasing airspeeds. The steepened gradients in the CC range ultimately lead to smaller changes in AoA for variations in lift coefficient and thus extend the airspeed range until the minimum AoA is reached. The calculated values for AoA are now positive for airspeeds close to stall speed. But the more interesting point is whether the aircraft achieves the necessary AoA above $\alpha > 3°$ at approach speed as defined in the CS-25.

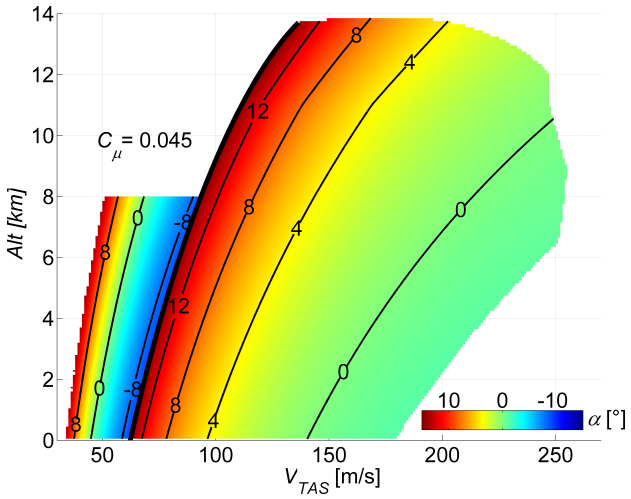

Figure 12: Approach configuration trim envelope with integrated droop nose (left) in CC area compared to the envelope of the cruise configuration (right) with MLW

This question might be answered multiple ways depending on the reference airspeed taken into account. For an AHLS aircraft the maximum lift can be manipulated by the variation of the air mass flow of the blowing system, which changes the resulting jet momentum coefficient. This also varies the stall speed, which is the reference for the minimum approach speed. Consequently the questions has to be answered whether the maximum or minimum achievable stall speed has to be used as a reference. If the minimum approach speed is calculated by the absolute minimum stall speed achievable with the AHLS at $C_\mu = 0.045$, the corresponding trimmed AoA would be positive and this way fulfill the requirement for almost neutral pitch attitudes during approach procedures. Table 3 shows the most relevant values of the described two cases and underlines the effectiveness of the DN application. The same values are given for $C_\mu = 0.033$ and the corresponding minimum approach speed. Nevertheless, this interpretation of the CS-25 does not seem to be reasonable, hence it raises the question of the applicability of the specification to AHLS supported civil aircraft.

A much more reasonable approach seems to be the comparison of AoA at the defined approach

speed for the aircraft with CN. The expected increase in AoA can be observed for this airspeed as well, but the impact of the droop nose on the resulting angles is not as high as initially hoped for. The results also reflect the influence of the DN on the lift slope gradient with respect to AoA. The integration of the DN barely affects this gradient for the BLC range of the system and therefore does not influence the resulting AoA effectively. For the CC range of the jet momentum the influence of the DN on this gradient is increased, which is reflected in the increased AoA for $C_\mu = 0.045$ at $V_{TAS} = 54\ \frac{\mathrm{m}}{\mathrm{s}}$. Anyhow the DN does not have sufficient impact to achieve the desired positive angles for this airspeed.

V_{TAS} $\left[\frac{m}{s}\right]$		α [°]	i_{HTP} [°]	α_{HTP} [°]	C_μ [−]
42	$V_{min,DN1}$	2.7	11.5	0.0	0.045
48	$V_{min,DN2}$	−3.3	10.3	0.0	0.033
54	$V_{min,CN}$	−5.9	7.6	−0.1	0.045
54	$V_{min,CN}$	−10	11	−0.1	0.033

Table 3: Approach configuration trim points with droop nose trim points for $X_{CG} = 19.5\%\ MAC$

Albeit that the newly calculated maximum lift coefficients and the resulting stall speeds stem from simplified conversions of 2D CFD data to 3D, this preliminary study shows that the aircraft's characteristics have improved but still do not allow to perform approaches according to the CS-25. Therefore the aerodynamic design has to be enhanced further to achieve the desired target area for the operational range of AoA. Modifying relative lengths of nose and main landing gear and adapting the wing's incidence angle can contribute to this aim, but are not seen as sufficient on their own.

6 Conclusions

Trim investigations have been carried out for a civil aircraft preliminary design that is employing an active high-lift system, specifically a blown Coandă flap. While trimmability is ensured and the resulting flight envelope for cruise is more than sufficient, the studies for approach and landing configurations suffer difficulties appearing through the application of the active high-lift system. Without any question the system achieves high lift values, but as a tradeoff the maximum angles of attack are reduced dramatically to values close to zero. The initial trim investigations show unacceptable ranges for angle of attack which are necessary to trim the aircraft for unaccelerated flight at approach speeds. The purpose of the investigated flap and AHLS setting as an approach flap setting thus is more than questionable. The requirement of the certification specification for large civil aircraft restricting the minimum approach speed to more than 23% above stall speed results in negative pitch attitudes for this aircraft configuration even in horizontal flight. The even larger pitch attitudes resulting from the addition of the negative flight path angle during approach are not acceptable as the necessary flare maneuver would be too extreme for civil transport.

It was tried to find a remedy by modifying the wing leading edge and keeping the used active high-lift system. The investigation of the combination of a droop nose with the Coandă flap delivered an increase in maximum angle of attack which, however, led to approach speed pitch attitude angles around zero only in some areas. Flying with considerable negative pitch attitude during approach does not seem manageable even considering adapted flight procedures or possibly control systems for pilot assistance.

The present paper shows the high relevance of flight mechanical considerations when active high-lift systems are applied to aircraft. It reveals the necessity to design the aircraft's aerodynamics within a defined target area which meets the flight mechanical requirements. This will be the next step in development in order to create a functional aircraft configuration. Being based on loss free aerodynamic data, the so found results will then need to be confirmed by further high-fidelity aerodynamic research in terms of droop nose application to the three-dimensional wing/body models and wind tunnel investigations. A subsequent task will be to analyze the dynamic behavior of the longitudinal motion of the aircraft analytically and numerically. As already mentioned, flight procedures and specifications need to be found to guarantee the aircraft's safety at all time. The reaction and recovery of an aircraft in during an AHLS failure remains unresolved. A complete failure of the system is expected to be catastrophic. Therefore it will be necessary to carry out extensive research on this topic. Regulatory issues (i.e. the applicability of specifications of conventional civil aircraft) need to be addressed as well; for example the question of the stall speed to be taken as the reference speed to define the minimum approach speed. In addition flying at very low speeds leads to the question if critical values for controllability could possibly need to be

defined alternatively. This could be used for the determination of a minimum approach speed which preserves enough controllability even though this speed would possibly be higher than the currently required 23% above stall speed.

The above considerations apart, it will be of interest to use the extremely high drag produced by the active high-lift system to introduce new steep approach procedures.

Acknowledgments

Financial support has been provided by the German Research Foundation (Deutsche Forschungsgemeinschaft - DFG) in the framework of the Sonderforschungsbereich 880. This work has been supported by the provison of particular CFD results created with VSAero by Tayson Weiss[4] for the clean wing/fuselage configuration and horizontal tailplane as well as DLR's Tau code by Dennis Keller[5] and Marco Burnazzi[6] for the full flaps configuration of the wing/fuselage combination with active high-lift system and wing leading edge devices. The reference aircraft design has been developed by Wolfgang Heinze[4] with PrADO.

References

[1] Werner-Westphal, C., W. Heinze, and P. Horst: *Multidisciplinary Integrated Preliminary Design Applied to Future Green Aircraft Configurations*. In *Aerospace Sciences Meetings*. American Institute of Aeronautics and Astronautics, Reno, NV, USA, January 2007.

[2] Keller, D.: *Numerical Investigation of the Longitudinal Static Stability of a Transport Aircraft with Circulation Control*. In *Proceedings of the 18th DGLR-STAB Symposium*, Stuttgart, Germany, 2012.

[3] Radespiel, R., K. C. Pfingsten, and C. Jensch: *Flow Analysis of Augmented High-Lift Systems*. Hermann Schlichting–100 Years, Notes on Numerical Fluid Mechanics and Multidisciplinary Design, 102:168–189, 2009.

[4] Pfingsten, K. C. and R. Radespiel: *Numerical simulation of a wing with a gapless high-lift system using circulation control*. New Results in Numerical and Experimental Fluid Mechanics, VI:71–79, 2008.

[5] Englar, R. J.: *Development of pneumatic aerodynamic devices to improve the performance, economics, and safety of heavy vehicles*. Technical Report SAE/TPS-2000-01-2208, Georgia Tech Research Institute, Atlanta, GA (US), Warrendale, PA, USA, 2000.

[6] Diekmann, J. H. and K.-U. Hahn: *Nonlinear Flight Dynamics Simulation Model for a Civil Aircraft with Active High Lift System*. In Radespiel, R. and R. Semaan (Eds.) (editors): *SFB 880 - Fundamentals of high-lift for future commercial aircraft, Biennial report*. Braunschweig, 2013.

[7] Gerhold, T.: *Overview of the Hybrid RANS Code TAU*. In Kroll, N. and J. Fassbender (editors): *MEGAFLOW – Numerical Flow Simulation for Aircraft Design*, volume 89 of *Notes on Numerical Fluid Mechanics and Multidisciplinary Design*, pages 81–92. Springer Verlag, Berlin Heidelberg, Germany, 2005.

[8] Schlichting, H. and E. Truckenbrodt: *Aerodynamik des Flugzeuges - Zweiter Band*. Springer Verlag, Berlin Heidelberg, Germany, 1969.

[9] Diekmann, J. H.: *Investigation of Flight Dynamics of a Civil Aircraft with Active High Lift System*. In *Proceedings of the 61st Deutscher Luft- und Raumfahrtkongress 2012*, Berlin, Germany, 2012.

[10] Diekmann, J. H.: *Nonlinear Flight Dynamics Simulation Model for a Civil Aircraft with Active High Lift System*. Institute report IB 111-2013/15, Institute of Flight Systems, DLR, Braunschweig, Germany, 2013.

[11] Schmidt, D. K.: *Modern Flight Dynamics*. McGraw-Hill, New York, 1st edition, 2012.

[12] EASA: *Certification Specification and Acceptable Means of Compliance for Large Aeroplanes CS-25*. Technical Report Amendment 13, European Aviation Safety Agency, June 2013.

[13] Burnazzi, M. and R. Radespiel: *Design of a droopnose configuration for a coanda active flap application*. In *Aerospace Sciences Meetings*. American Institute of Aeronautics and Astronautics, January 2013. http://dx.doi.org/10.2514/6.2013-487.

[4] Institute of Aircraft Design and Lightweight Structures (IFL), TU Braunschweig

[5] Institute of Aerodynamics and Flow Technology (AS), German Aerospace Center (DLR)

[6] Institute of Fluid Mechanics (ISM), TU Braunschweig